ELSEVIER

Journal of Nuclear Materials 244 (1997) 278–294

journal of nuclear materials

The effect of alloy composition on radiation-induced segregation in Fe–Cr–Ni alloys

T.R. Allen [a,*], G.S. Was [a], E.A. Kenik [b]

[a] *Department of Nuclear Engineering and Radiological Sciences, The University of Michigan, Ann Arbor, MI 48109, USA*
[b] *Metals and Ceramics Division, Oak Ridge National Laboratory, Oak Ridge, TN 37831, USA*

Received 5 February 1996; accepted 20 August 1996

Abstract

The effect of alloy composition on radiation-induced segregation (RIS) was investigated in austenitic iron-base and nickel-base alloys using proton irradiation. Specifically, RIS was studied by irradiation of Ni–18Cr, Ni–18Cr–9Fe, and Fe–20Cr–9Ni over a dose range of 0 to 1.0 dpa and a temperature range of 200 to 500°C. Grain boundary composition was measured using Auger electron spectroscopy and scanning transmission electron microscopy with energy dispersive X-ray spectroscopy. Measurements from this study along with measurements from Fe–16Cr–24Ni, Fe–20Cr–24Ni, Fe–24Cr–24Ni, and Fe–24Cr–19Ni alloys irradiated with protons confirm that RIS is strongly dependent on the alloy composition. Trends in segregation behavior in Fe-base alloys are consistent with high temperature diffusion measurements, indicating that a vacancy mechanism is the most likely primary driving force for RIS in austenitic steels. The migration energy for Cr is shown to be larger than the migration energy of Fe. Segregation measurements in Ni-base alloys are not consistent with high temperature diffusion measurements, indicating that ordering forces may be significant in the segregation process. Comparison of model calculations to measured RIS data indicate that Fe, Cr, and Ni diffusivities are composition dependent. This dependence on alloy composition limits the predictive ability of simple models because of the need for separate diffusion parameters for every alloy composition.

1. Introduction

Because of the potential deleterious effects on nuclear reactor structural materials, radiation-induced segregation (RIS) in austenitic stainless steels has been studied for quite some time [1]. Segregation has been measured using both Auger electron spectroscopy (AES) [2] and scanning transmission electron microscopy with energy dispersive X-ray spectroscopy (STEM/EDS) [3] on materials irradiated with neutrons [3,6], electrons [4], heavy ions [5] and protons [2]. A review of RIS in binary and ternary alloys is given in Ref. [7]. Since RIS occurs at low temperature (200–600°C in proton irradiated stainless steels), segregation measurements provide information on low energy kinetics that are not measurable at the high temperatures where diffusion coefficients are normally measured (greater than 1000°C). By measuring the rates of segregation of Fe, Cr, and Ni as a function of bulk alloy composition, information about the interactions between atoms in the alloy can be determined. Improving the understanding of the basic interactions that drive the segregation process will lead to an improved ability to predict segregation in a range of austenitic alloys under a variety of irradiation conditions.

1.1. Analyzing RIS in ternary alloys

Radiation-induced segregation occurs when a local point defect flux causes a net flux of atoms toward or away from the grain boundary. The atom flux depends on the diffusivity of each constituent (which describes the rate at which an atom will interact with the point defect flux) and on the local composition. For example, the flux of Cr atoms due

* Corresponding author. E-mail: goober@engin.umich.edu.

PII S0022-3115(96)00744-1

to the vacancy flux is a function of the local Cr concentration C_{Cr} and the Cr diffusivity, d_v^{Cr}:

$$J_v^{Cr} = f\left(C_{Cr}, d_v^{Cr}\right). \tag{1}$$

Therefore, if *either* the concentration or the diffusivity changes, the flux (and therefore the amount of segregation) will change. Concentration changes with no corresponding change in diffusivity (random alloy effects) can still change the amount of segregation. The diffusivity has two components, a constant pre-exponential term d_0 and a migration energy term E_{vm}^{Cr}:

$$d_v^{Cr} = d_0^{Cr} \exp\left(\frac{-E_{vm}^{Cr}}{kT}\right). \tag{2}$$

If either the pre-exponential term or the migration energy changes as a function of bulk alloy composition, the diffusivity will change and therefore cause changes in segregation. The key to understanding the dependence of segregation on bulk alloy concentration is to determine the composition dependence of the diffusivities.

Studies have shown that major element composition affects void swelling in Fe–Cr–Ni alloys [8,9]. Composition dependent diffusivities were suggested by Venker and Erlich [10] as being important in determining the swelling behavior of Fe–Cr–Ni alloys. A major goal in this study is to determine the dependence of diffusivities on bulk composition. This can be accomplished by investigating the rate at which Cr, Fe, and Ni deplete or enrich at the grain boundary. Data can be plotted as the ratio of the *magnitude* of the change in Cr concentration (unirradiated grain boundary Cr minus irradiated grain boundary Cr) to the *magnitude* of the change in Ni concentration (unirradiated grain boundary Ni minus irradiated grain boundary Ni) ($|\Delta Cr/\Delta Ni|$). This ratio indicates the fraction of grain boundary sites occupied by Ni that were previously occupied by Cr. A ratio of 1 indicates that every Cr that leaves the boundary is replaced by a Ni (with Fe neither enriching or depleting). A value of 0.5 indicates that for two Ni atoms arriving at the boundary, one Cr leaves (and therefore one Fe leaves). The term 'Cr–Ni replacement rate' will be used to denote this ratio. The Cr–Ni replacement rate is determined by the relative amounts of grain boundary segregation. The segregation is determined by the relative atomic fluxes. The relative fluxes are determined by the diffusivities. Therefore, the Cr–Ni replacement rate provides information on the relative diffusivities of each constituent in the alloy.

The segregation could also be described using the Fe–Ni replacement rate ($|\Delta Fe/\Delta Ni|$), which is related to the Cr–Ni replacement rate since:

$$Cr + Fe + Ni = 1 \quad \text{or} \quad \frac{\Delta Cr}{\Delta Ni} + \frac{\Delta Fe}{\Delta Ni} = -1. \tag{3}$$

The Cr–Ni replacement rate was chosen because Cr always depletes and Ni always enriches in Fe–Cr–Ni alloys. Therefore, the major changes are captured using $|\Delta Cr/\Delta Ni|$.

The segregation in an Fe–Cr–Ni system is determined by the ratios of the diffusivities d_{vm}^{Cr}/d_{vm}^{Ni}, d_{vm}^{Fe}/d_{vm}^{Ni} and d_{vm}^{Cr}/d_{vm}^{Fe}. In irradiated Fe–Cr–Ni alloys, Cr always depletes and Ni always enriches at grain boundaries. In most alloys, Fe depletes at grain boundaries. Therefore, if the segregation is driven by the vacancy flux, Cr must be the fastest diffuser and Ni the slowest diffuser in the system:

$$\frac{d_{vm}^{Cr}}{d_{vm}^{Ni}} > \frac{d_{vm}^{Fe}}{d_{vm}^{Ni}} > 1. \tag{4}$$

Fe will enrich or deplete depending on the Fe diffusivity relative to the average diffusivity in the alloy. If the Fe diffusivity is greater than the average diffusivity in the alloy, Fe will deplete. If the Fe diffusivity is less than the average diffusivity in the alloy, Fe will enrich. The Ni enriched at the boundary occupies positions previously occupied by either Cr or Fe. The amount of Cr and Fe depletion is determined by the Cr/Fe diffusivity ratio d_{vm}^{Cr}/d_{vm}^{Fe}.

Fig. 1 demonstrates the effect of relative diffusivity on grain boundary segregation. Predictions using the Perks RIS model [11] for the grain boundary Cr concentration are plotted versus model predicted grain boundary Ni concentration. The model calculations are for an Fe–20Cr–24Ni alloy irradiated at 400°C to various doses. As the dose increases, the grain boundary Cr depletes and the grain boundary Ni enriches. Five different calculations are shown, each assuming a different ratio of the Cr-to-Fe diffusivity (d_{vm}^{Cr}/d_{vm}^{Fe}). As the Cr-to-Fe diffusivity increases from 1.3 to 2.1, the change in grain boundary Cr concentration (ΔCr) increases, and the change in grain boundary Ni concentration (ΔNi) decreases. Therefore, the Cr–Ni replacement rate ($|\Delta Cr/\Delta Ni|$) increases as the Cr-to-Fe diffusivity increases. The Cr–Ni replacement rate is a measure of the relative diffusivities. Studying the Cr–Ni replacement rate as a function of alloy composition can provide information about the relative diffusivities as a function of alloy composition.

To study segregation behavior as a function of bulk alloy composition, a variable that relates segregation behavior to composition must be chosen. The sum of all atomic concentrations in the alloy must equal one. Therefore, the flux of Cr and Fe away from the boundary must equal the flux of Ni to the boundary:

$$J_{Cr} + J_{Fe} = -J_{Ni}. \tag{5}$$

The amount of Cr segregation is determined by the fraction of Cr flux relative to the total flux away from the boundary (flux of Cr plus Fe). This fraction can be expressed:

$$\frac{J_{Cr}}{J_{Cr} + J_{Fe}} = \frac{C_{Cr} d_{Cr}}{C_{Cr} d_{Cr} + C_{Fe} d_{Fe}}. \tag{6}$$

If the Cr and Fe diffusivities were equal then the flux ratio in Eq. (6) equals the ratio of the concentrations:

$$\frac{J_{Cr}}{J_{Cr}+J_{Fe}} = \frac{C_{Cr}}{C_{Cr}+C_{Fe}}. \tag{7}$$

If $d_{vm}^{Cr} = d_{vm}^{Fe}$, then at small $C_{Cr}/(C_{Cr}+C_{Fe})$, the Cr–Ni replacement rate would be small. At large $C_{Cr}/(C_{Cr}+C_{Fe})$, the Cr–Ni replacement rate would be large. If $d_{vm}^{Cr} \neq d_{vm}^{Fe}$, then a plot of the Cr–Ni replacement rate as a function of bulk $C_{Cr}/(C_{Cr}+C_{Fe})$ will have curvature. These relationships are shown in Fig. 2. The Cr–Ni replacement rate increases with $C_{Cr}/(C_{Cr}+C_{Fe})$ if $d_{vm}^{Cr} = d_{vm}^{Fe}$ and has a curvature if $d_{vm}^{Cr} \neq d_{vm}^{Fe}$. The curvature is specific to the relationship between d_{vm}^{Cr} and d_{vm}^{Fe}. Therefore, the ratio $C_{Cr}/(C_{Cr}+C_{Fe})$ will be used throughout this paper to designate different alloy compositions.

For Fe–Cr–Ni alloys, experimental high temperature diffusion measurements indicate that Cr is the fastest diffuser and Ni the slowest diffuser for Cr concentrations from 0 to 30 wt% and with Ni concentrations from 19 to 87 wt% [12]. High temperature diffusion occurs via a vacancy mechanism. Therefore, if the primary driving mechanism for RIS in ternary Fe–Cr–Ni alloys is a coupling with the vacancy flux, we expect Cr to always deplete and Ni to always enrich at grain boundaries. Fe will either enrich or deplete depending on the segregation kinetics for Fe (relative to Cr and Ni) and the amount of Fe in the alloy. The diffusivities used to model RIS in austenitic Fe–Cr–Ni alloys have not been directly measured and are typically inferred from high temperature diffusion coefficient measurements. The diffusivity of Cr (d_{vm}^{Cr}) is related to the diffusion coefficient for Cr (D_{Cr}) by the following expression:

$$D_{Cr} = d_{vm}^{CR} C_v, \tag{8}$$

where C_v is the equilibrium vacancy concentration. If the measured segregation is consistent with model predictions that use diffusivities derived from high temperature diffusion measurements (which are driven only by vacancy flux), then RIS can be assumed to be driven primarily by a vacancy mechanism. If the measured segregation is inconsistent with model predictions that use diffusivities derived from high temperature diffusion measurements, then either the relative diffusivities of Cr, Ni, and Fe are different at irradiation temperatures or a significant contribution to the segregation comes from differences in solute coupling with the interstitial flux.

1.2. Measurements of RIS in Fe–Cr–Ni systems

Few studies have examined the dependence of major element RIS on bulk alloy composition in Fe–Cr–Ni alloys. Dumbill [6] studied a series of Fe-base alloys with constant Cr and varying Ni, irradiated with neutrons to low dose. For a range of 15–30 wt% Ni with constant Cr of 18 wt%, the magnitude of the Cr depletion decreased with increasing bulk Ni concentration. For these samples, the sample preparation prior to the irradiation produced a significant grain boundary Cr enrichment. After the low dose irradiation, the Cr profiles were 'W' shaped with enriched grain boundaries and depletion in the planes adjacent to the grain boundary. Cr depletion was measured

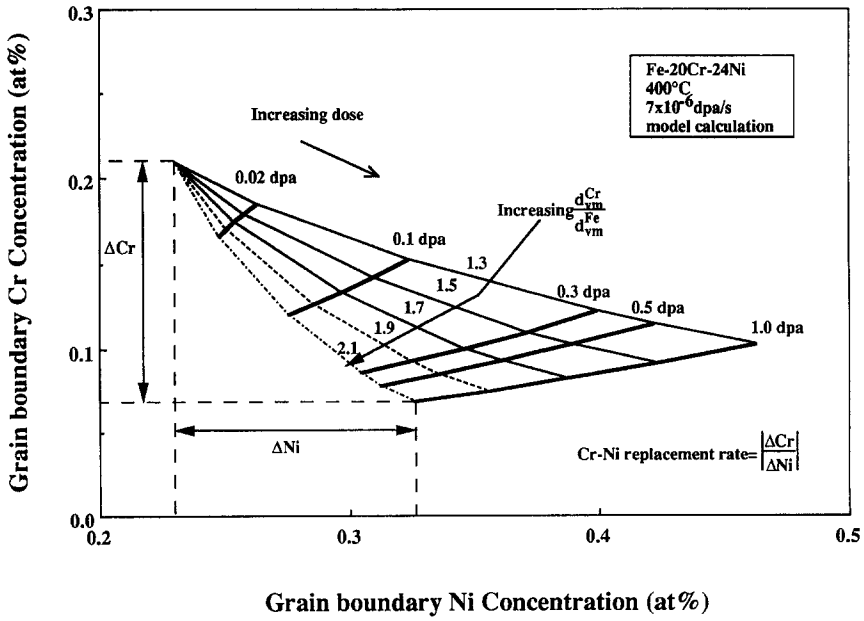

Fig. 1. Model calculations indicate how changing diffusivities alter the predicted segregation. Increasing the Cr–Fe diffusivity ratio increases the Cr depletion and decreases the Ni enrichment.

as the difference between bulk and the minimum Cr concentration in the profile (which did not correspond to the grain boundary). For those samples irradiated to higher dose, no solution treatment Cr enrichment remained. For these higher dose samples, the amount of Cr segregation increased with Ni concentration in the range studied. Dumbill and Williams [3] found that Cr depletion in 15 wt% Ni alloys irradiated with neutrons is independent of Cr concentration (in the range of 10–20 wt% Cr). The Cr segregation in 35 wt% Ni alloys was smaller than in the 15 wt% Ni alloys. Damcott et al. [2] irradiated a series of Fe–Cr–Ni alloys with protons at 400°C. An Fe–xCr–24Ni (x = 16, 20, 24 at%) series irradiated to 1 dpa showed greater Cr depletion and less Ni enrichment with increasing bulk Cr content. Additionally, an Fe–20Cr–xNi (x = 9, 24 at%) series and an Fe–24Cr–xNi (x = 19, 24 at%) series were irradiated to 1 dpa. Both the Fe–20Cr–xNi (x = 9, 24 at%) and the Fe–24Cr–xNi (x = 19, 24 at%) showed increasing Cr depletion and Ni enrichment with increasing bulk Ni concentration. Attempts to model the segregation behavior using the Perks model for RIS [11] indicated that composition dependent diffusivities were required to accurately model the trends of the data, most notably in the Fe–xCr–24Ni series. Finally, Watanabe et al. [4] irradiated an Fe–15Cr–xNi series (x = 15, 20, 25, 30, 35, 40) with electrons at 450°C to 7.2 dpa. Segregation measurements showed a peak in Ni enrichment in the alloys with about 30 at% bulk Ni. Cr depletion increased slightly with increasing bulk Ni concentration. Modeling calculations using the inverse Kirkendall effect with constant diffusivities for all alloy compositions indicated a peak in Ni segregation between 15–20 at% depending on irradiation dose. No attempt was made to calculate the predicted segregation using alloy dependent diffusivities.

The dependence of RIS on alloy composition for Fe-base alloys is shown in Fig. 3. The fractional Ni change ((grain boundary Ni-bulk Ni)/bulk Ni) as a function of bulk Cr/(Cr + Fe) ratio from the work of Damcott et al. [2] (AES measurements), Dumbill and Williams [3] (STEM/EDS measurements), and Watanabe et al. [4] (STEM/EDS measurements) is plotted. With the exception of the Fe–xCr–35Ni material irradiated with neutrons [3], Ni enrichment decreases with increasing bulk Cr/(Cr + Fe) ratio. The magnitude of Ni enrichment is clearly influenced by alloy composition. This dependence of segregation on alloy composition can be investigated to provide information on the relative diffusivities of Fe, Cr, and Ni in Fe–Cr–Ni alloys. In this work, the dependence of RIS on bulk alloy composition in austenitic Fe–Cr–Ni alloys is studied. Ni–18Cr, Ni–18Cr–9Fe and Fe–20Cr–9Ni alloys have been irradiated with protons, and grain boundary concentrations were measured using AES and STEM/EDS. Segregation data from Fe-base alloys irradiated with protons [2], electrons [4], and neutrons [3,6] are also included in the analysis. Segregation data will be analyzed to show that significant differences in diffusivi-

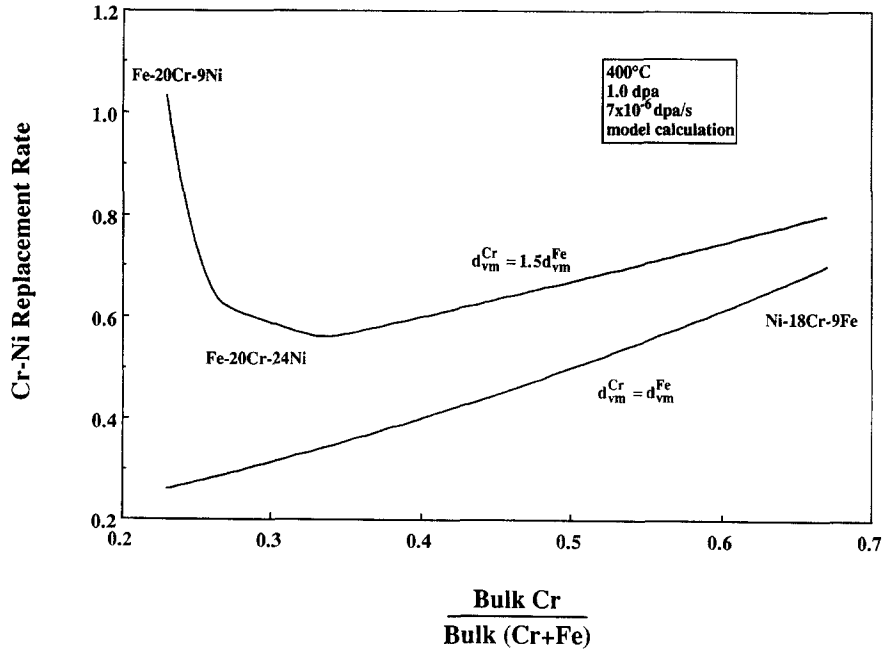

Fig. 2. The effect of diffusivity on Cr–Ni replacement rate. If the Cr diffusivity equals the Fe diffusivity, the Cr–Ni replacement rate increases with composition. If the Cr diffusivity does not equal the Fe diffusivity, the Cr–Ni replacement rate is a complicated function of alloy composition.

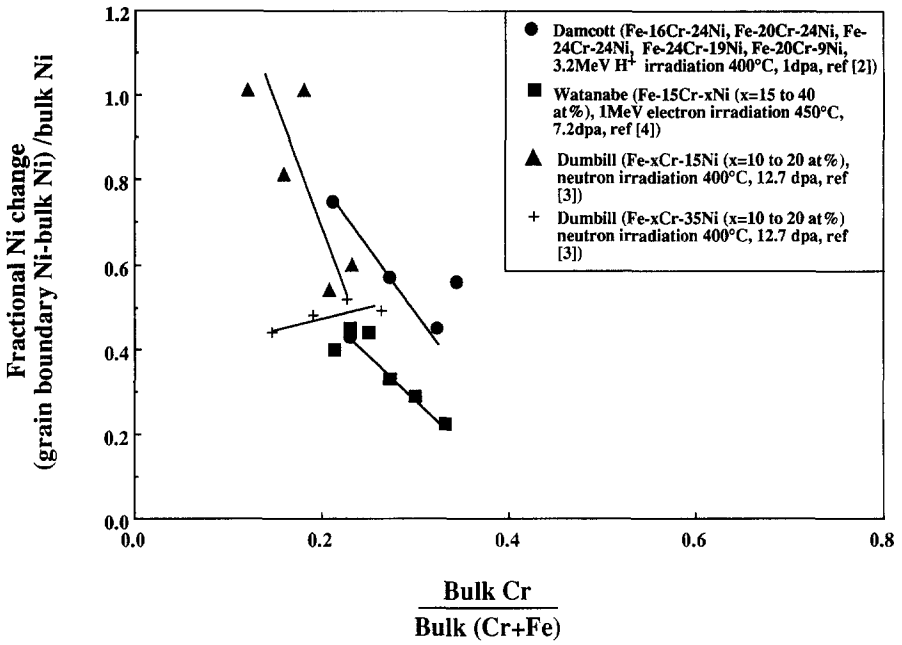

Fig. 3. Comparison of Ni segregation in proton (400°C, 1 dpa), electron (450°C, 7.2 dpa), and neutron irradiated (400°C, 12.7 dpa) Fe–Cr–Ni alloys. Ni segregation is dependent on alloy composition.

ties as a function of alloy composition must exist to explain the trends of the measured segregation data.

2. Experimental procedure

Irradiations of Ni–18Cr, Ni–18Cr–9Fe, and Fe–20Cr–9Ni alloys were conducted using 3.2 MeV protons at an ion flux of 6.25×10^{13} cm^{-2} s^{-1}, resulting in a nearly uniform damage rate of approximately 7×10^{-6} dpa/s through the first 35 μm of the proton range (45 μm). Table 1 gives the bulk compositions of these alloys as measured using electron microprobe analysis. Details of the sample preparation procedure, irradiation technique, and grain boundary measurement techniques are given in Ref. [13]. Grain boundary composition was measured in the Ni–18Cr and the Ni–18Cr–9Fe alloys which were irradiated at temperatures between 200 and 500°C at 100°C intervals to a dose of 0.5 dpa and at 400°C to accumulated damage levels of 0.1, 0.3, 0.5, and 1.0 dpa. Grain boundary composition was also measured in the Fe–20Cr–9Ni alloy which was irradiated at 400°C to final doses of 0.1 and 1.0 dpa. Unirradiated grain boundaries were characterized in the Ni–18Cr–9Fe, Ni–18Cr, and Fe–20Cr–9Ni alloys to determine the grain boundary chemistry prior to the irradiation.

Grain boundary microchemical analysis was performed using AES in a Perkin-Elmer PHI 660 Scanning Auger Microprobe and using STEM/EDS. The STEM/EDS was performed on a Phillips EM400T/FEG at Oak Ridge

Table 1
Summary of bulk alloy compositions in atomic percent (second line gives normalized compositions for Fe + Cr + Ni = 100%)

Alloy	Cr	Ni	Fe	Mn	Mo	Si	C	N	P	S
Ni–18Cr	18.24	81.74	0	0	0.002	0	0.005		0.006	0.004
	18.24	81.76	0							
Ni–18Cr–9Fe	18.26	72.36	9.32	0.010	0.002	0.027	0.014		0.007	0.004
	18.26	72.40	9.33							
Fe–20Cr–9Ni	20.72	8.88	69.16	1.11	< 0.01	0.09	0.021	0.012	0.01	< 0.009
	20.97	8.99	70.04							

Table 2
Inputs to the Perks Model

Input parameter	Notation	Value	Reference
Vacancy jump frequency for Fe	ω_{FeV}	2.8×10^{13} s^{-1}	[15]
Vacancy jump frequency for Cr	ω_{CrV}	5.0×10^{13} s^{-1}	[15]
Vacancy jump frequency for Ni	ω_{NiV}	1.5×10^{13} s^{-1}	[15]
Fe-vacancy correlation factor	f_{FeV}	0.785	[15]
Cr-vacancy correlation factor	f_{CrV}	0.668	[15]
Ni-vacancy correlation factor	f_{NiV}	0.872	[15]
Interstitial jump frequency	ω_I	1.5×10^{12} s^{-1}	[11]
Atom-interstitial correlation factor	f_I	0.44	[16]
Vacancy migration energy for Fe	E_{vm}^{Fe}	1.3 eV	[17]
Vacancy migration for Cr	E_{vm}^{Cr}	1.3 eV	[17]
Vacancy migration energy for Ni	E_{vm}^{Ni}	1.3 eV	[17]
Interstitial migration energy	E_{Im}	0.9 eV	[18]
Vacancy formation energy	E_{fv}	1.9 eV	[19]
Dislocation density	ρ	1×10^{14} m^2	[20]
Recombination volume	Z	12	FCC lattice
Thermodynamic factor	α	1	[19]

Table 3
Summary of AES segregation measurements

Alloy	Temp. (°C)	Dose (dpa)	Iron (at%)	Chromium (at%)	Nickel (at%)	Measurements	Samples	Irradiations
Ni–18Cr	200	0.5	—	14.6 ± 1.3	85.4 ± 1.3	28	2	1
Ni–18Cr	300	0.5	—	11.5 ± 1.4	88.5 ± 1.4	33	2	1
Ni–18Cr	400	0.5	—	10.1 ± 1.6	89.9 ± 1.6	62	5	3
Ni–18Cr	500	0.5	—	12.9 ± 2.3	87.1 ± 2.3	23	2	1
Ni–18Cr–9Fe	200	0.5	6.7 ± 2.0	15.7 ± 0.6	77.6 ± 2.0	16	1	1
Ni–18Cr–9Fe	300	0.5	5.4 ± 1.7	13.8 ± 1.0	80.8 ± 2.1	14	1	1
Ni–18Cr–9Fe	400	0.5	5.8 ± 1.6	13.5 ± 1.2	80.7 ± 2.4	27	2	1
Ni–18Cr–9Fe	500	0.5	6.5 ± 1.9	15.7 ± 1.1	77.8 ± 2.9	30	2	1
Ni–18Cr	—	0.0	—	17.1 ± 0.7	82.9 ± 0.7	12	1	NA
Ni–18Cr	400	0.1	—	13.4 ± 1.7	86.6 ± 1.7	33	2	1
Ni–18Cr	400	0.3	—	11.8 ± 1.4	88.2 ± 1.4	32	2	1
Ni–18Cr	400	1.0	—	10.6 ± 1.9	89.4 ± 1.9	36	2	2
Ni–18Cr–9Fe	—	0.0	9.3 ± 1.0	17.9 ± 1.3	72.8 ± 1.6	12	2	—
Ni–18Cr–9Fe	400	0.1	5.1 ± 1.0	14.1 ± 1.1	80.8 ± 1.2	23	2	1
Ni–18Cr–9Fe	400	0.3	4.9 ± 1.2	13.9 ± 1.7	81.1 ± 1.9	23	2	1
Ni–18Cr–9Fe	400	1.0	5.5 ± 1.8	13.8 ± 1.6	80.7 ± 3.0	29	2	2
Fe–20Cr–9Ni	—	0.0	68.7 ± 1.2	23.2 ± 1.5	8.1 ± 0.5	12	1	—
Fe–20Cr–9Ni	400	0.1	69.4 ± 1.0	21.4 ± 1.4	9.2 ± 0.8	25	2	1
Fe–20Cr–9Ni	400	1.0	70.3 ± 1.3	17.0 ± 1.7	12.7 ± 1.3	65	5	3

Table 4
Summary of STEM-EDS segregation measurements

Alloy	Temp. (°C)	Dose (dpa)	Iron (at%)	Chromium (at%)	Nickel (at%)	Measurements	Samples	Irradiations
Ni–18Cr	—	0.0	—	18.8 ± 0.6	81.2 ± 0.6	15	1	—
Ni–18Cr	400	0.1	—	15.7 ± 1.0	84.3 ± 1.0	22	2	2
Ni–18Cr	400	0.3	—	14.3 ± 1.5	85.7 ± 1.5	34	2	1
Ni–18Cr	400	0.5	—	13.0 ± 1.6	87.0 ± 1.6	33	2	2
Ni–18Cr	400	1.0	—	13.6 ± 1.0	86.4 ± 1.0	15	1	1
Ni–18Cr–9Fe	—	0.0	9.2 ± 0.2	17.9 ± 0.7	72.8 ± 0.8	17	1	—
Ni–18Cr–9Fe	400	0.1	6.6 ± 0.6	16.0 ± 0.9	77.4 ± 1.4	22	2	1
Ni–18Cr–9Fe	400	0.3	5.8 ± 0.5	15.4 ± 0.7	78.7 ± 1.0	18	1	1
Ni–18Cr–9Fe	400	0.5	5.4 ± 1.0	14.4 ± 1.3	80.2 ± 2.2	45	2	1
Ni–18Cr–9Fe	400	1.0	5.8 ± 0.7	15.3 ± 0.8	78.7 ± 1.2	20	1	1

National Laboratory with an incident probe width of 2 nm. The experimental doses and dose rates reported throughout this paper are calculated using NRT [14] theory assuming a displacement energy of 25 eV. Model calculations were performed using the Perks model [11]. Unless specifically stated otherwise, the input parameters used in the Perks model are given in Table 2. Model calculations are corrected for the fraction of point defects that escape the collision cascade and are free to migrate through the lattice [21]. A value of 0.2 was used as the freely migrating defect fraction for proton irradiations. Additionally, when comparing model calculations to Auger data, the model calculations are convoluted with the Auger escape depth so that the model calculation can be directly compared to the Auger measurement.

3. Results

The grain boundary segregation measurements for each temperature and dose combination are summarized in Table

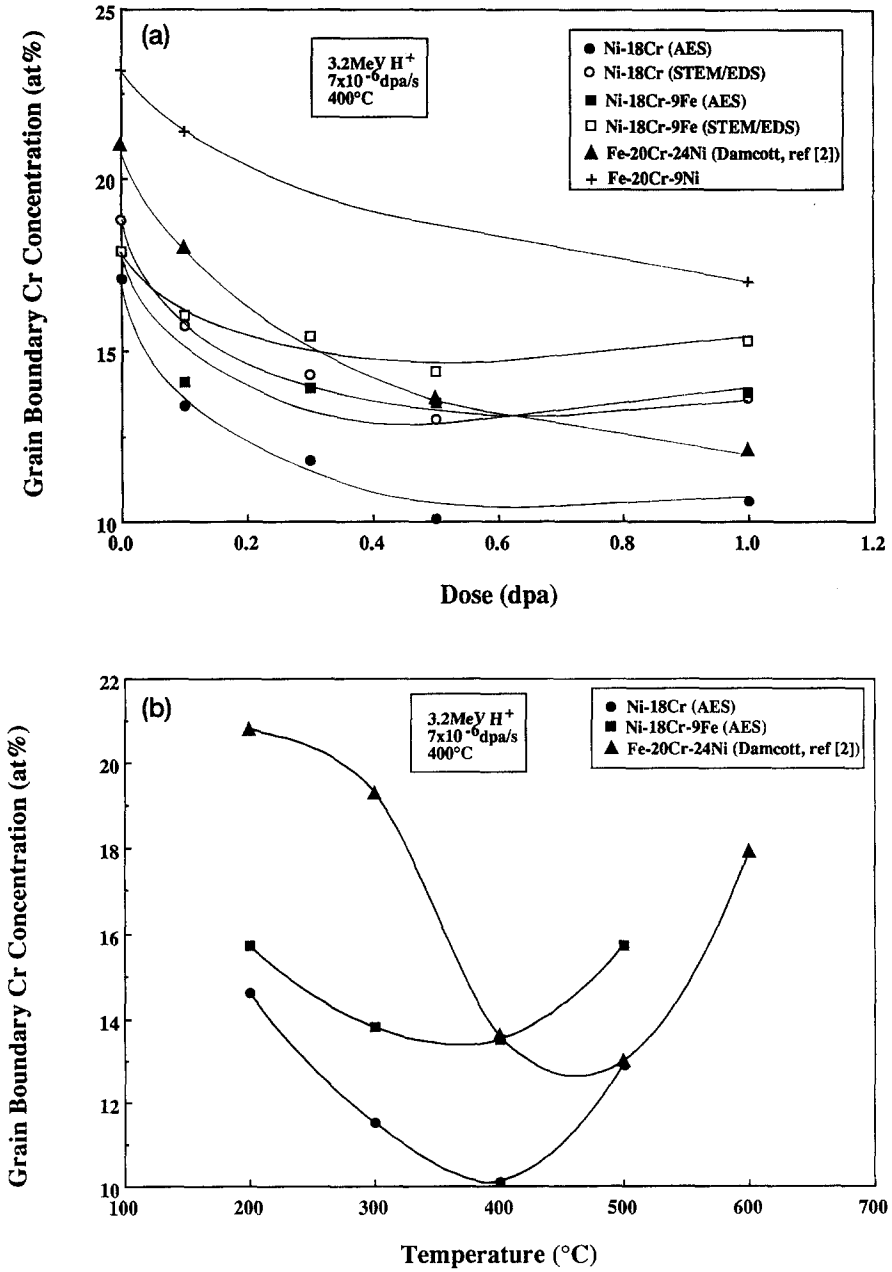

Fig. 4. (a) Grain boundary Cr measurements as a function of dose for alloys irradiated with 3.2 MeV protons at 400°C. (b) Grain boundary Cr measurements as a function of temperature for alloys irradiated with 3.2 MeV protons to 0.5 dpa.

3 (AES measurements) and Table 4 (STEM/EDS measurements). The uncertainty listed for each average is the standard deviation of all the measurements for the given experimental temperature and dose. Cr depletes and Ni enriches at the grain boundary in all three alloys. Fe depletes in the Ni–18Cr–9Fe and enriches slightly in the Fe–20Cr–9Ni alloy. Good agreement exists between the segregation measured using both AES and STEM/EDS in both Ni–18Cr and Ni–18Cr–9Fe. AES measurements typically indicate a grain boundary Cr concentration about 1–2 at% less than STEM/EDS measurements. This is consistent with Carter et al. [22] who measured RIS in proton irradiated stainless steels and Walmsley et al. [23] who measured RIS in neutron irradiated stainless steels

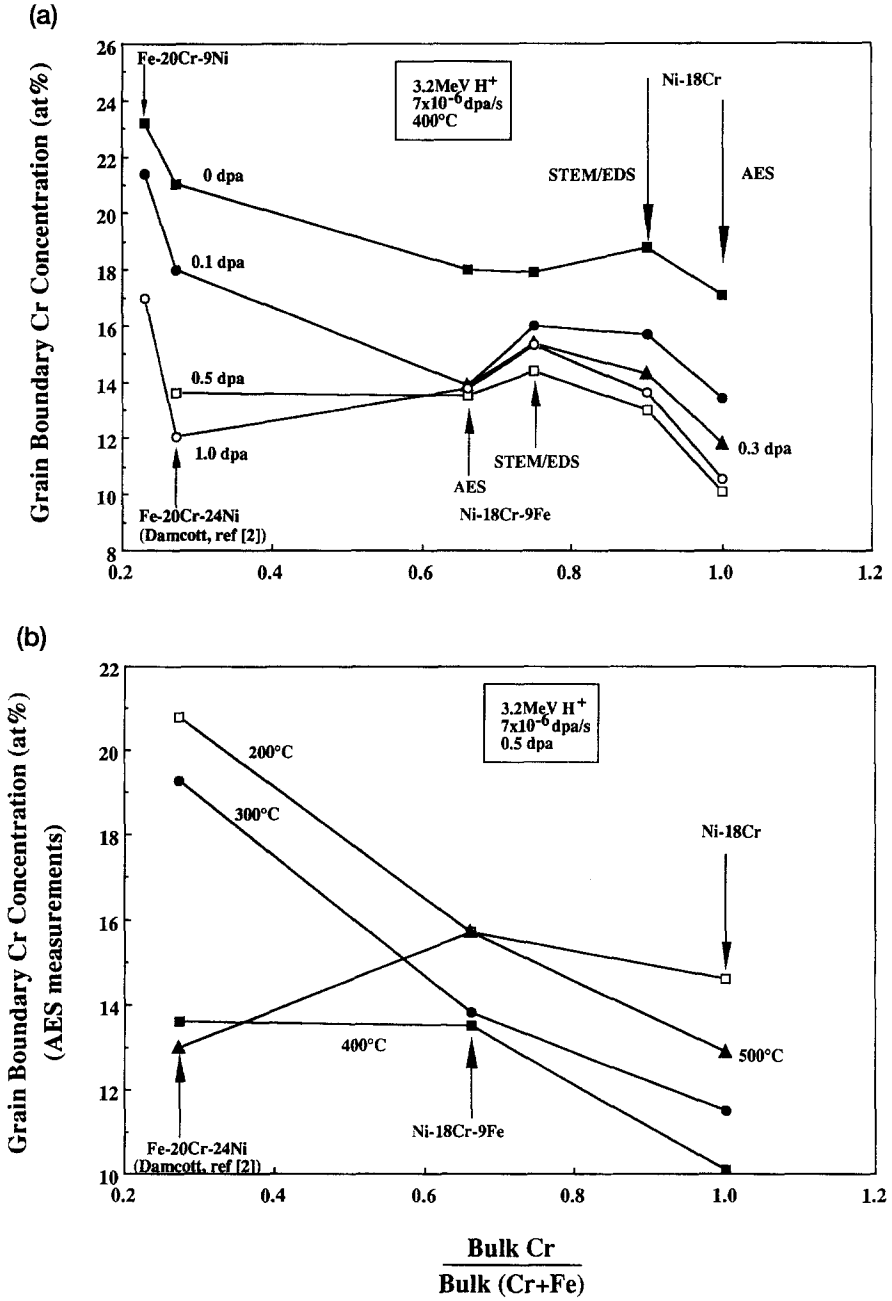

Fig. 5. (a) Grain boundary Cr measurements as a function of composition for alloys irradiated with 3.2 MeV protons at 400°C to varying dose. (b) Grain boundary Cr measurements (AES) as a function of composition for alloys irradiated with 3.2 MeV protons to 0.5 dpa at varying temperatures.

and found a similar difference between AES and STEM/EDS measurements.

The dependence of segregation on bulk alloy composition as a function of temperature and dose is shown in Figs. 4 and 5. Included on the figures are grain boundary Cr concentrations from an Fe–20Cr–24Ni alloy as measured by Damcott et al. [2]. Fig. 4a and b plot the grain boundary Cr concentration as a function of dose and temperature, respectively. Each alloy approaches steady-state at a different rate and each alloy has a minimum Cr concentration at a different temperature. In Fig. 5a, the Cr concentration as a function of bulk $C_{Cr}/(C_{Cr} + C_{Fe})$ ratio is plotted for various doses with each data symbol representing an irradiation dose. Each bulk alloy has a unique segregation behavior. For example, the Cr concentration at 1.0 dpa in the Fe–20Cr–24Ni alloy is lower than in the Fe–20Cr–9Ni alloy. The grain boundary Cr concentration in the Ni–18Cr alloy irradiated to 1.0 dpa is around 3 at% less than the grain boundary Cr concentration in the Ni–18Cr–9Fe alloy irradiated to 1.0 dpa. In Ni–18Cr–9Fe, Fe depletes, reducing the amount of Cr depletion at the grain boundary relative to the Ni–18Cr alloy. The dependence of segregation on bulk alloy composition for several irradiation temperatures is also shown in Fig. 5b. Once again, each bulk alloy has a unique segregation behavior, with the minimum Cr concentration occurring at different temperatures. Therefore, measurements from alloys irradiated with protons clearly indicate that grain boundary segregation depends on bulk composition, in agreement with RIS studies from materials irradiated with neutrons and electrons.

4. Discussion

The RIS measurements from this study and from the works outlined in the introduction clearly indicate that RIS is composition dependent. Having shown that grain boundary segregation depends on composition, the following questions remain: (1) Does the irradiating particle type have an effect on the segregation kinetics? (2) Can differences in composition (with fixed values of diffusivities regardless of alloy composition) explain the trends in the segregation data or must the diffusivities be a function of composition to explain the measured segregation data? Additionally, if the diffusivities are composition dependent, are diffusivities inferred from the RIS measurements consistent with diffusivities inferred from high temperature diffusion measurements? (3) Can information about migration energies be determined from the temperature dependence of the segregation? (4) Finally, if the diffusivities inferred from RIS measurements are not consistent with those measured in high temperature diffusion measurements, what alters the driving force for segregation? Each of these questions will be answered in the following sections.

4.1. Relationship between segregation kinetics and irradiating particle type

The type of irradiating particle is not expected to affect the trends in segregation as a function of alloy composition. The changes in RIS should be consistent regardless of irradiating species. This assumption can be tested by comparing Cr–Ni replacement rates as a function of alloy composition from different experiments (irradiating particle, temperature, and dose). Segregation measurements on a series of constant Cr, varying Ni, alloys have been performed by Dumbill [6] (Fe–18Cr–xNi–0.5Si–2.5Mo and Fe–18Cr–xNi–0.5Si, where $x = 15$ to 30 at%), Watanabe et al. [4] (Fe–15Cr–xNi where $x = 15$ to 40 at%), and Damcott et al. [2] (Fe–20Cr–xNi, where $x = 9$, 24 at%). The Ni–18Cr–9Fe and Fe–20Cr–9Ni alloys in this work, along with the Fe–20Cr–24Ni alloy from Damcott, gives a series of alloys with constant Cr concentration near 20 at% and Ni concentration varying from 9 to 72 at%. The Cr–Ni replacement rate for these constant Cr, varying Ni alloys (irradiated at temperatures from 400–450°C) is plotted in Fig. 6. For bulk $C_{Cr}/(C_{Cr} + C_{Fe})$ ratios less than about 0.3 (all the Fe-base alloys), the Cr–Ni replacement rates measured in the alloys irradiated with protons and neutrons decrease as the bulk $C_{Cr}/(C_{Cr} + C_{Fe})$ ratio increases. The Cr–Ni replacement rates measured in the alloys irradiated with electrons increase as the bulk $C_{Cr}/(C_{Cr} + C_{Fe})$ ratio increases. The Cr–Ni replacement decreases slightly in going from Fe–20Cr–24Ni to Ni–18Cr–9Fe alloys irradiated with protons. The RIS measurements for constant Cr, varying Ni alloys indicate that Cr–Ni replacement rates for the temperature range of 400–450°C are alloy specific and that trends in Cr–Ni replacement rates with changing alloy composition are, in general, consistent for alloys irradiated with neutrons and protons. Therefore, the segregation kinetics are similar in both proton and neutron irradiations.

Segregation measurements on a series of constant Ni, varying Cr, alloys have been performed by Dumbill and Williams [3] (Fe–xCr–15Ni and Fe–xCr–35Ni, where $x = 10$ to 20 at%) and by Damcott et al. [2] (Fe–xCr–24Ni, where $x = 16$, 20, 24). The Cr–Ni replacement rate for these constant Cr, varying Ni alloys (for a temperature range of 400–450°C) is plotted in Fig. 7. Cr–Ni replacement rate data from the spinodal decomposition of an Fe–7.5Cr–35Ni irradiated with neutrons (450°C, 12.5 dpa) [24] is also included on the figure. As bulk $C_{Cr}/(C_{Cr} + C_{Fe})$ ratios increase, the Cr–Ni replacement rate increases for all the segregation data. The RIS measurements for constant Ni, varying Cr alloys indicate Cr–Ni replacement rates are alloy specific. Trends in Cr–Ni replacement rates with changing alloy composition are, in general, consistent across all of the irradiation conditions analyzed, and therefore, using either protons or neutrons do not affect the segregation kinetics. The segregation is determined by the bulk composition and/or the relative diffusivities of Fe,

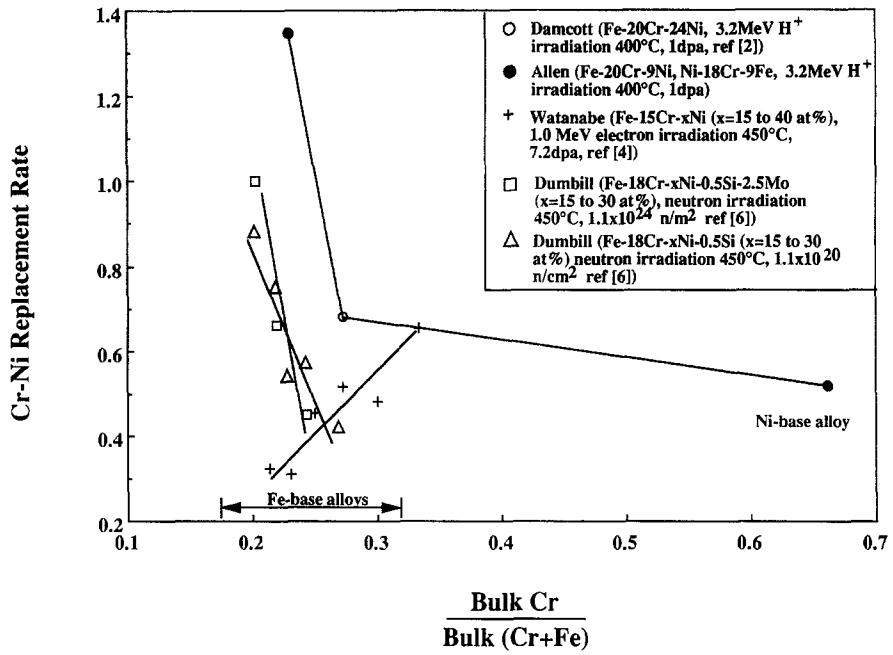

Fig. 6. Cr–Ni replacement rate at grain boundaries for constant Cr, varying Ni alloys.

Cr, and Ni. The next section will discuss how to determine if diffusivities vary with alloy composition.

4.2. Composition dependent diffusivities

Given that RIS is significantly affected by bulk alloy composition, the cause of the different segregation behavior must be determined. As noted in the introduction, variations in composition and in diffusivities (as composition varies) will change the amount of segregation. By comparing model calculations to AES measurements, diffusivities will be shown to be alloy specific. Additionally, the observed diffusivities in the Fe-base alloys are consistent with high temperature diffusion coefficient measure-

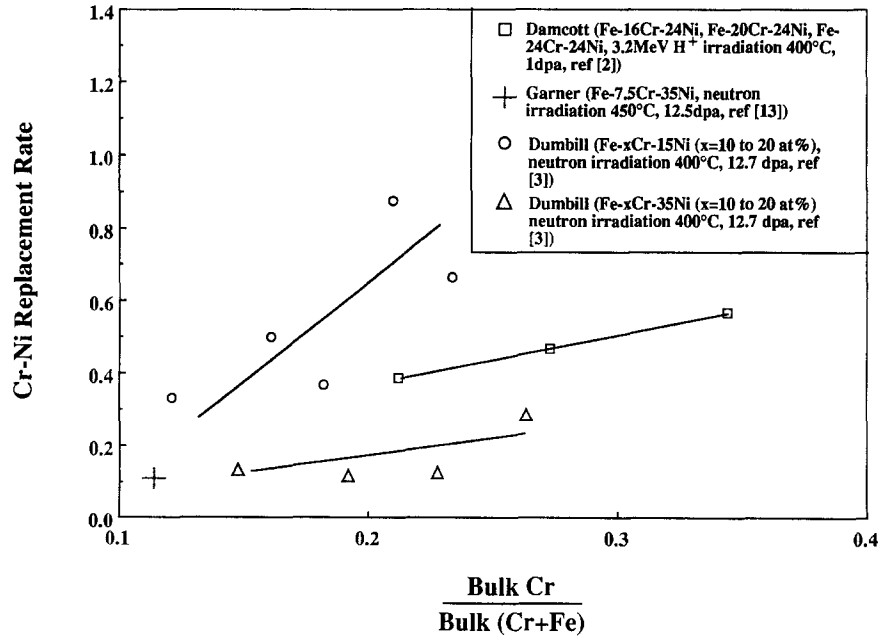

Fig. 7. Cr–Ni replacement rate at grain boundaries for constant Ni, varying Cr alloys.

ments and therefore the primary driving force for segregation is most likely the vacancy flux. Diffusivities in Ni–18Cr–9Fe are not consistent with high temperature diffusion measurements. Therefore, the driving force for segregation in Ni–18Cr–9Fe is more complex, indicating that the driving force for segregation is more complicated than simple inverse Kirkendall behavior.

The method for analyzing the composition dependence of the diffusivities is to compare model calculations which assume constant diffusivity (regardless of bulk composition) to segregation measurements to determine if diffusivities depend on alloy composition. If the measured Cr–Ni replacement rates follow the trends of model predictions (using constant diffusivities), then the diffusivities are independent of alloy composition. If the measured Cr–Ni replacement rates do not follow the trends of model predictions (using constant diffusivities), then the diffusivities are alloy specific. If diffusivities are shown to be alloy specific, we can then compare diffusivities inferred from the RIS measurements to those inferred from high temperature diffusion coefficient measurements. If the measured Cr–Ni replacement rates are consistent with model predictions which use diffusivities derived from high temperature diffusion coefficient measurements (which are driven only by vacancy flux), then RIS can be assumed to be driven primarily by a vacancy mechanism. If the measured segregation is inconsistent with model predictions that use diffusivities derived from high temperature diffusion measurements, then either the relative diffusivities of Cr, Ni, and Fe are different at irradiation temperatures, or a significant contribution to the segregation comes from differences in solute coupling with the interstitial flux.

Cr–Ni replacement rates calculated from segregation data are compared to Cr–Ni replacement rates calculated from model predictions for both constant Cr, varying Ni, and constant Ni, varying Cr, alloys. Model calculations are performed using the Perks model [11], which assumes that only the vacancy flux contributes to the grain boundary segregation (no differences in interstitial jump rates). Unless otherwise specified, migration energies are assumed equal for Fe, Cr, and Ni and differences in diffusivities are assumed to occur as differences in pre-exponential factors. Constant diffusivity ratios of $d^{Cr}_{vm}/d^{Ni}_{vm} = 2.55$, $d^{Fe}_{vm}/d^{Ni}_{vm} = 1.67$, and $d^{Cr}_{vm}/d^{Fe}_{vm} = 1.53$ are used for the constant diffusivity calculations for all alloys. These diffusivity ratios are based on the diffusion coefficient ratios measured by Rothman et al. [15] for an Fe–15Cr–20Ni alloy and have traditionally been used in RIS calculations for stainless steels.

The most comprehensive set of alloy-dependent segregation measurements are those of Damcott et al. [2], who measured the grain boundary concentrations using AES in Fe-base alloys irradiated with protons at 400°C for a variety of alloy compositions. One series was a constant Ni, varying Cr (Fe–xCr–24Ni, with $x = 16$, 20, and 24 at%), alloys. A second series was constant Cr, varying Ni (Fe–24Cr–xNi, with $x = 24$ and 19 at%). The final series was another constant Cr, varying Ni (Fe–20Cr–xNi, with $x = 9$ and 24 at%). The Ni–18Cr–9Fe and Ni–18Cr alloys irradiated in this work extend the final series to give four alloys with Cr near 20 at% and Ni of 9, 24, 72 and 82 at%. A comparison of model predicted and measured Cr–Ni replacement rates from the Fe–xCr–24Ni ($x = 16$, 20, 24 at%) series are plotted in Fig. 8. Constant diffusivity model calculations indicate that with increasing Cr concentration, the rate of Cr–Ni replacement at the boundary will increase slightly just due to composition differences. The data show a steeper increase in Cr–Ni replacement rate with increasing Cr concentration than do the constant diffusivity calculations. Therefore, the ratio of Cr-to-Fe diffusivity must increase with increasing Cr concentration. This increase in Cr-to-Fe diffusivity is consistent with the high temperature diffusion coefficients of Rothman who showed that for a constant Ni system, the Cr-to-Fe diffusion coefficient ratio increases with increasing Cr concentration. Alloy specific diffusivities, inferred from diffusion coefficients (D_{Cr}/D_{Fe}) from Rothman et al. [15] are listed on Fig. 8 for reference. For two of the three alloys, the calculations using the diffusivities based on the high temperature diffusion measurements of Rothman more accurately predict the measured segregation than the constant diffusivity calculations.

The alloy dependence of the segregation is also shown in Fig. 9 which plots the Cr–Ni replacement rates from constant diffusivity model calculations against AES data for the Fe–24Cr–xNi ($x = 19$, 24 at%) alloy series. The constant diffusivity model calculations predict a small decrease in the Cr–Ni replacement rates with increasing Ni concentration. As with the varying Cr system, the AES data shows a larger change in Cr–Ni replacement rate than the constant diffusivity model calculations. This behavior is consistent with Rothman's high temperature diffusion data which shows a decreasing Cr-to-Fe diffusion coefficient ratio with increasing Ni and constant Cr. Model calculations using alloy specific diffusivity ratios based on Rothman's data follow the trends of the data much better than do those using constant diffusivity ratios.

The composition dependence of diffusivities is also confirmed by analyzing a constant Cr, varying Ni system. The segregation data from the Fe–20Cr–24Ni alloy irradiated by Damcott et al. [2] combined with the data from Fe–20Cr–9Ni and Ni–18Cr–9Fe from this work is included in the analysis to give a series of alloys with Cr near 20 at% and Ni ranging from 9 to 72 at%. The Cr–Ni replacement rates from model calculations and AES measurements are shown in Fig. 10. The constant diffusivity model predictions indicate a minimum Cr–Ni replacement rate at a bulk $C_{Cr}/(C_{Cr} + C_{Fe})$ ratio near 0.3 and increasing Cr–Ni replacement rates at high and low Ni concentrations. As with the Fe–24Cr–xNi series, the measurements from the two Fe-base alloys show a larger decrease in Cr–Ni replacement rate with increasing Ni concentration

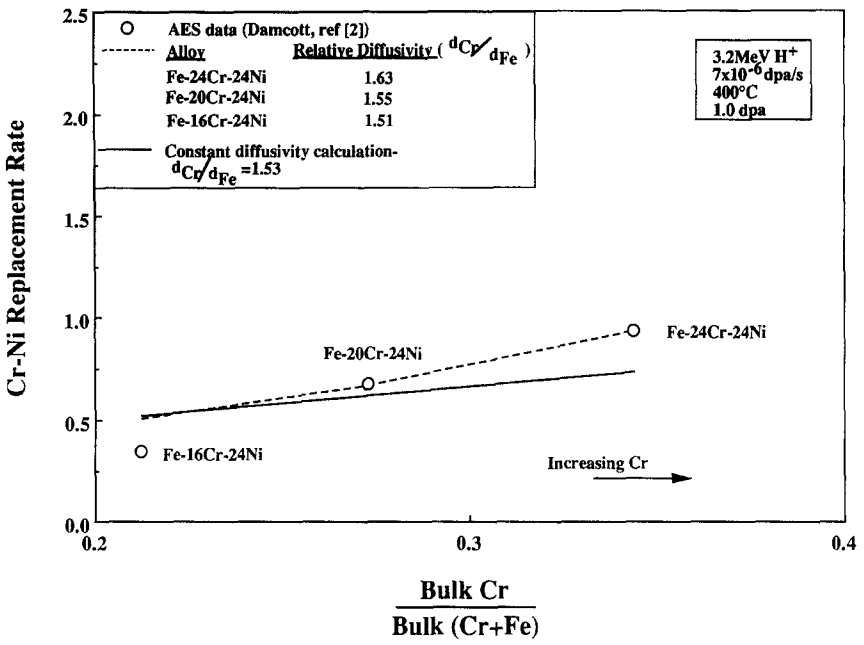

Fig. 8. Cr–Ni replacement rate at grain boundaries for a series of constant Ni, varying Cr alloys (Fe–xCr–24Ni, x = 16, 20, 24) irradiated with protons at 400°C to 1.0 dpa. Calculations using alloy specific diffusivities (from Ref. [15]) more accurately follow the trends of the AES measurements.

than the constant diffusivity calculations, which is indicative of decreasing Cr-to-Fe diffusivity ratios. Rothman's high temperature diffusion data also indicated a decreasing Cr-to-Fe diffusivity with increasing Ni concentration, although the calculation using the Cr-to-Fe diffusivity extrapolated from Rothman's work predicts a Cr–Ni replacement rate that is larger than the experimental data. The behavior of the Ni–18Cr–9Fe alloy is more complicated.

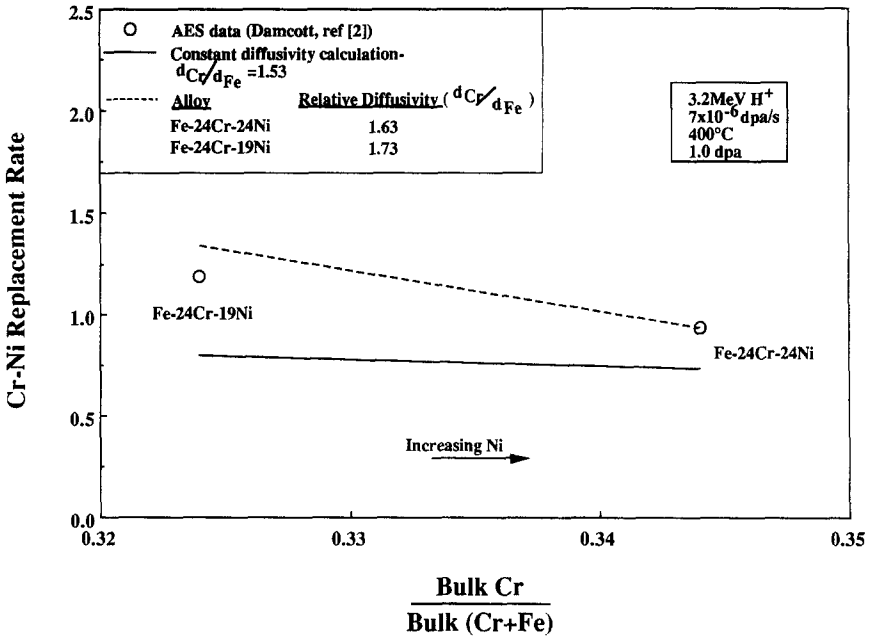

Fig. 9. Cr–Ni replacement rate at grain boundaries for a series of constant Cr, varying Ni alloys (Fe–24Cr–xNi, x = 19, 24 at%) irradiated with protons at 400°C to 1.0 dpa. Calculations using alloy specific diffusivities (from Ref. [15]) more accurately follow the trends of the AES measurements.

When comparing the Fe–20Cr–24Ni and the Ni–18Cr–9Fe alloys, constant diffusivity calculations indicate that the Cr–Ni replacement rate should increase with increasing Ni concentration, but the Cr–Ni replacement rate calculated from the AES data actually decreases. The trends from the model predictions and from the data move in opposite directions. Model calculations using alloy specific diffusivities are plotted for each alloy and show better agreement with the Fe-base data but worse agreement with the Ni–18Cr–9Fe data. High temperature diffusion coefficient data indicates that the Cr-to-Fe diffusion coefficient ratio (and therefore the diffusivity ratio) is larger in the Ni–18Cr–9Fe alloy (1.64) [12] than in the Fe–20Cr–24Ni alloy (1.55) [15], shifting the Cr–Ni replacement rate predicted by the model farther from the rate determined from the data. Thus, the Ni–18Cr–9Fe segregation data is not consistent with the high temperature diffusion data. In irradiated Ni–18Cr–9Fe, Cr diffuses slower and Fe diffuses faster than expected from high temperature diffusion coefficient measurements. The comparison of model calculations and AES data for the 20Cr–xNi series confirms that alloy specific diffusivities are required to accurately predict measured segregation. Segregation in Fe-base alloys is consistent with the predictions of the high temperature diffusion data, while segregation in the Ni-base alloy is not consistent with high temperature diffusion data.

In summary, the analysis of RIS data from Fe–Cr–Ni alloys clearly shows that to properly describe the segregation behavior, alloy specific diffusivities must be used. Measured segregation data indicates that for Fe-base alloys, increasing Cr concentration at constant Ni causes the Cr-to-Fe diffusivity ratio to increase. For alloys with constant Cr, increasing the Ni concentration causes the Cr-to-Fe diffusivity ratio to decrease. Segregation trends in the Fe-base alloys are consistent with trends in high temperature diffusion measurements, indicating that the segregation is most likely driven by vacancy (inverse Kirkendall) effects. Segregation trends in the Ni–18Cr–9Fe alloy are not consistent with trends in high temperature diffusion measurements, indicating a difference in diffusivity between high and low temperature. The segregation in the Ni–18Cr–9Fe alloy will be discussed in more detail later in the discussion.

4.3. Temperature dependence of segregation shows Fe, Cr, Ni migration energies unequal

The temperature dependence of RIS in Fe–20Cr–24Ni and Ni–18Cr–9Fe provides information concerning the migration energies. Relative diffusivities will be shown to be a function of temperature, and therefore migration energies for Fe, Cr, and Ni are not equal. Information about the migration energies of Cr and Fe can be deduced from the Cr–Ni replacement rate at the grain boundaries as a function of temperature. Fig. 11 plots the Cr–Ni replacement rate calculated from measured data for the Fe–20Cr–

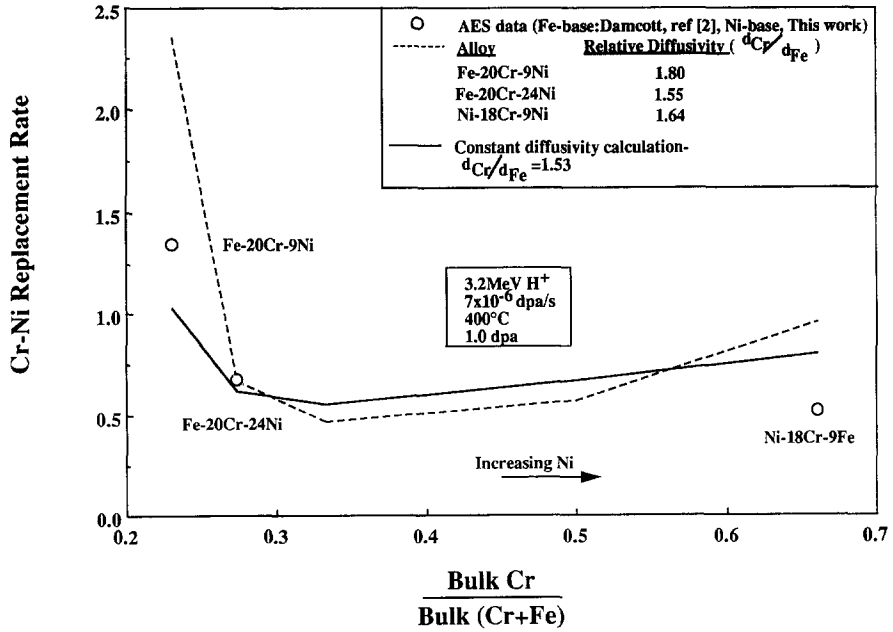

Fig. 10. Cr–Ni replacement rate at grain boundaries for a series of constant Cr, varying Ni alloys (Fe–20Cr–xNi, $x = 9$, 24, 72 at%). irradiated with protons at 400°C to 1.0 dpa. Calculations using alloy specific diffusivities (from Ref. [15,12]) more accurately follow the trends of the AES measurements for Fe-base alloys, but not for the Ni-base alloy.

24Ni and Ni–18Cr–9Fe alloys irradiated to 0.5 dpa (the AES measurement for the Fe–20Cr–24Ni alloy at 200°C was irradiated to 1 dpa) as a function of irradiation temperature. Also plotted are the Cr–Ni replacement rates calculated from model predictions which assume equal migration energies (1.30 eV) for each element in the alloy. The calculations are for a 0.5 dpa irradiation to correspond to each of the data points (the calculation for the Fe–20Cr–24Ni alloy irradiated at 200°C is for 1 dpa).

With increasing temperature, the model predicted Cr–Ni replacement rates decrease slightly for both alloys, opposite those determined from measurements. At higher temperatures, measurements show that Cr is more likely to exchange with Ni at the grain boundary. Since the temperature dependence of the migration rates is determined by the migration energies, the Cr-vacancy migration energy must be larger than the Fe-vacancy migration energy in the Fe–20Cr–24Ni alloy. This is consistent with earlier work [25] that showed that RIS modeling of the Fe–20Cr–24Ni alloy is more accurate if the Cr migration energy is slightly larger than that of Fe. The Cr–Ni replacement rate derived from the AES measurements in the Ni–18Cr–9Fe is fairly constant. Therefore, Cr is exchanging more rapidly with Ni than the model calculations indicate. The Cr-vacancy migration energy must be larger than the Fe migration energy in the Ni–18Cr–9Fe alloy. Based on the smaller difference between model calculation and measurements, the migration energies of Fe and Cr appear to be closer in the Ni–18Cr–9Fe alloy. Comparison of the temperature dependence of the Cr–Ni replacement rate calculated from model predictions and from grain boundary measurements indicate that the migration energies of Fe and Cr are *not* equal in either Fe–20Cr–24Ni or Ni–18Cr–9Fe. The Cr migration energy is larger than the Fe migration energy ($E_{vm}^{Cr} > E_{vm}^{Fe}$), with the difference being larger in Fe–20Cr–24Ni.

4.4. Short range ordering effects on segregation in Ni–18Cr–9Fe

Segregation in the Ni–18Cr–9Fe alloy was the only case investigated where the segregation was not consistent with high temperature diffusion measurements. Additionally, the approach to steady-state is very rapid, much faster than in other alloys studied. Fig. 4a plotted the segregation as a function of dose for four different alloys, clearly showing the rapid approach to steady-state in the Ni–18Cr–9Fe alloy. In this section, the rate of Cr segregation will be shown to be much smaller than expected from high temperature diffusion measurements. Analysis of this behavior shows that segregation may be affected by short range ordering forces.

The anomalous segregation of Cr and Fe in the Ni–18Cr–9Fe alloy is apparent by comparing the dose-dependent behavior of segregation with that of Fe–20Cr–24Ni. Fig. 12a shows the magnitude of the rate at which Cr is replaced by Ni at the grain boundary (|dCr/dNi|) as a function of dose for Fe–20Cr–24Ni irradiated with protons at 400°C. |dCr/dNi| is calculated both from model predictions and from AES data. Model calculations were performed using the Perks model and assume that only the vacancy flux contributes to the grain boundary segregation

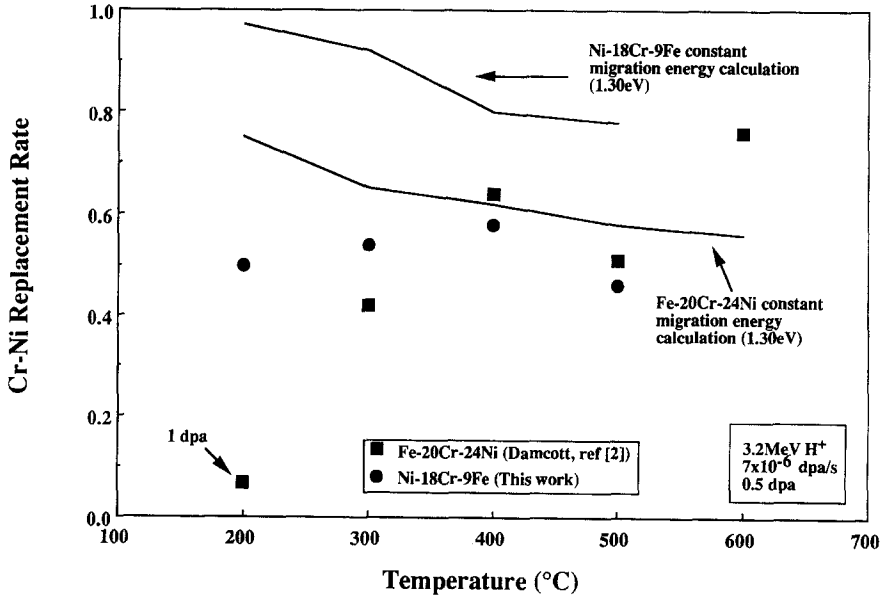

Fig. 11. Cr–Ni replacement rate at grain boundaries for an Fe–20Cr–24Ni alloy and for a Ni–18Cr–9Fe alloy irradiated with protons to 0.5 dpa. The data has a temperature dependence not predicted by the calculations, indicating a difference in migration energies between Cr and Fe.

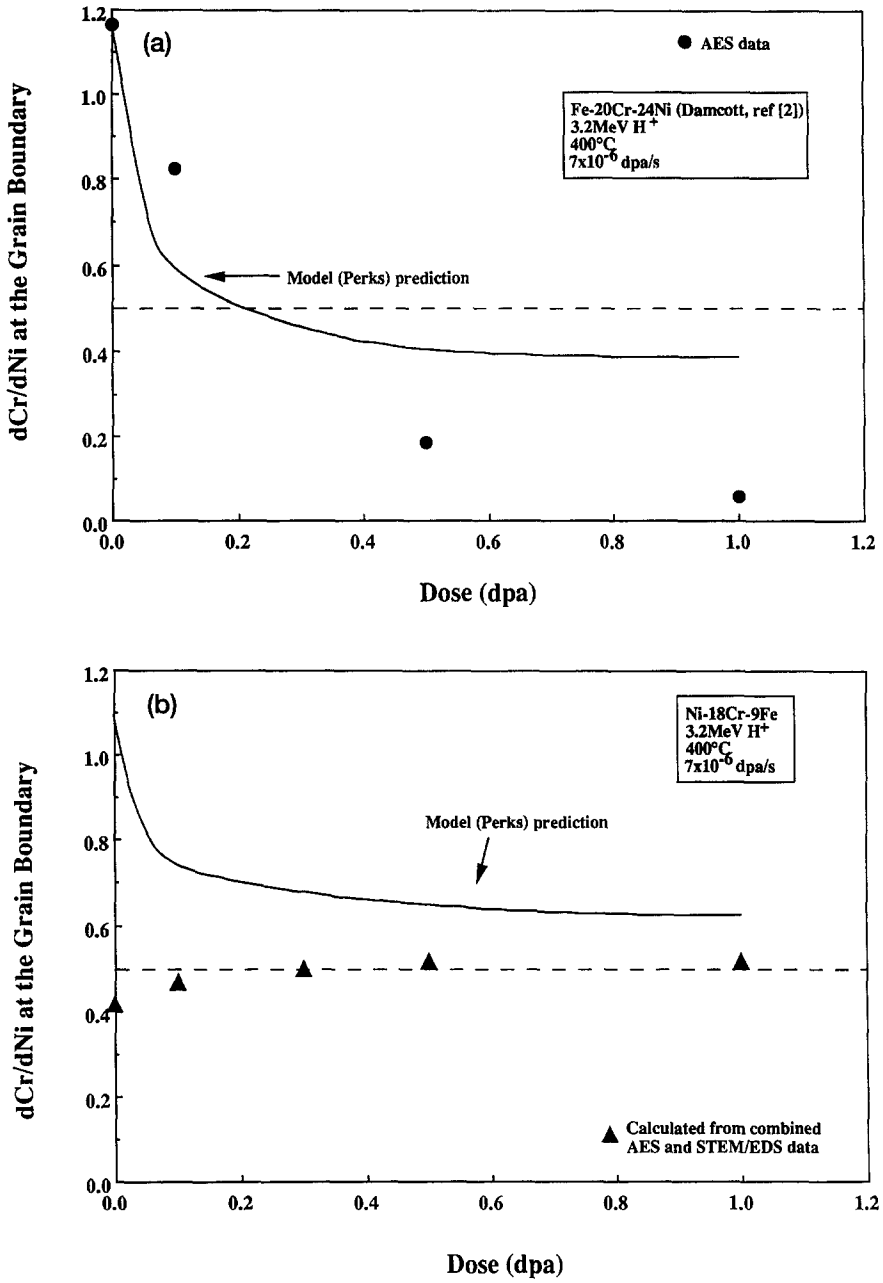

Fig. 12. (a) Calculation of the rate of change of Cr with respect to Ni at the grain boundary for an Fe–20Cr–24Ni alloy irradiated at 400°C. dCr/dNi is calculated from model predictions and also from AES data. (b) Calculation of the rate of change of Cr with respect to Ni at the grain boundary for a Ni–18Cr–9Fe alloy irradiated at 400°C. dCr/dNi is calculated from model predictions and also from AES and STEM data.

(no differences in interstitial jump rates). From the model predictions in Fig. 12a, as dose increases, Cr is replaced by Ni at a smaller rate. The dashed line at $|dCr/dNi| = 0.5$ indicates the point where half the Ni arriving at the boundary are filling positions previously occupied by Cr (the other positions being previously occupied by Fe). Above the line, the majority of atoms leaving the boundary are Cr. At low dose, Cr leaves the boundary at a high rate. At higher doses, when the Cr at the boundary is sufficiently depleted, Cr is no longer dominant in exchanging with Ni. The $|dCr/dNi|$ calculated from *model predictions*, for which the Fe–20Cr–24Ni alloy is equal to 0.5 (equal Cr and Fe replacement rates with Ni), occurs at a dose just larger than 0.2 dpa. The $|dCr/dNi|$ calculated from *AES*

data, for which the Fe–20Cr–24Ni alloy is equal to 0.5 (equal Cr and Fe replacement rates with Ni), occurs at a dose just about 0.2 dpa. The measured replacement rates of Cr with Ni in the Fe–20Cr–24Ni alloy are consistent with the model calculations.

In contrast, the Cr–Ni replacement rate for the Ni–18Cr–9Fe alloy is *not* consistent with model predictions, as shown in Fig. 12b. The |dCr/dNi| calculated from *model predictions* never reaches 0.5. Comparing the Fe–20Cr–24Ni and Ni–18Cr–9Fe calculations in Fig. 12a and b, which assume the diffusivities for Fe–20Cr–24Ni and Ni–18Cr–9Fe are equal, Cr–Ni replacements are always expected to be dominant in the Ni-base alloy, which has a larger bulk Cr-to-Fe ratio (2:1) than the Fe–20Cr–24Ni alloy (1:3). In contrast to the model predictions, |dCr/dNi| calculated from AES and STEM data moves in the opposite direction of |dCr/dNi| calculated from model predictions. The RIS data indicates that early in the irradiation, Cr is replaced by Ni at a much smaller rate than expected from calculation (indicating that Fe is replaced by Ni at a much higher rate than expected). At later stages in the irradiation, Cr and Fe are replaced with Ni at nearly equal rates. The measurements indicate that Fe diffuses at about the same rate as Cr in the Ni–18Cr–9Fe alloy, contrary to high temperature diffusion measurements [12] which show Cr to be the faster diffuser.

A possible explanation for the anomalous segregation behavior in the Ni–18Cr–9Fe alloy is strong short range ordering forces which may accelerate the segregation process in the Ni–18Cr–9Fe alloy. Many measurements have shown ordering to occur in Fe–Cr–Ni alloys, with strong ordering around the Ni–18Cr–9Fe composition. Cenedese et al. [26], using neutron diffuse scattering, observed a tendency to form short range Ni–Cr pairs in an Fe–23Cr–21Ni alloy. Marwick et al. [27], using both electron microscopy and Mossbauer spectroscopy, studied the effect of adding Cr to an ordered Ni_3Fe lattice. This study of $(Ni_3Fe)_{1-x}Cr_x$ alloys determined that Cr additions rapidly reduce the long range order of Ni_3Fe. The long range order is replaced by a state of short range order. The Cr tends to occupy iron sites in an ordered Ni_3Fe lattice, with Cr atoms surrounded by a Ni-rich shell and the formation of separate Fe-rich regions. The formation of Ni–Cr pairs was more likely than the formation of Ni–Fe pairs. Marucco [28] studied variations in lattice parameter, electrical resistivity, and microhardness in a series of ternary Fe–Cr–Ni alloys (30–67 at% Ni, 17–32 at% Cr, 1–51 at% Fe) and found that short range ordering increases with increasing Ni and decreasing Fe. Dimitrov et al. [29] studied the isochronal annealing of excess resistivity following electron irradiation of various Fe–16Cr–xNi alloys and found that the excess resistivity associated with short range order due to vacancy motion increased significantly with increasing Ni concentration. The tendency to form Ni–Cr pairs may slow down the Cr segregation relative to the Fe. In the Ni–18Cr–9Fe alloy, this tendency to order would not be seen in high temperature diffusion measurements as the small ordering forces would not be significant at high temperature. Short range ordering forces that tend to form Ni–Cr pairs may explain the anomalous segregation behavior seen in the Ni–18Cr–9Fe alloy.

5. Conclusions

Radiation-induced segregation in Fe–Cr–Ni alloys has been shown to be dependent on alloy composition. The data indicates that the diffusivities for Fe, Cr, and Ni change with alloy composition. The segregation in Fe-base alloys follows the trends predicted by high temperature diffusion measurements and thus indicates that the atom-vacancy exchange is the most likely driving mechanism for segregation. The migration energy of Cr is shown to be larger than the migration energy of Fe. Segregation in a Ni-base ternary alloy does not follow the predictions of high temperature diffusion measurements. The diffusion may be influenced by short range ordering forces known to exist in high Ni content Fe–Cr–Ni alloys. The dependence of the diffusivity on alloy composition limits the predictive ability of simple models because of the need for separate diffusion parameters for every alloy composition. Future modeling efforts of RIS in Fe–Cr–Ni alloys need to account for the variation in relative diffusivity to correctly model grain boundary segregation behavior.

Acknowledgements

The authors gratefully acknowledge P.L. Andresen at the General Electric Company for supplying the sample alloys and the bulk chemical analysis. We are grateful to R.D. Carter, J.M. Cookson, and D. Damcott for assistance in performing sample irradiations and to the Michigan Ion Beam Laboratory at the University of Michigan for the use of the irradiation facilities. We thank M. Atzmon for his helpful critique of the work. We also thank the Surface Analysis Laboratory at the Ford Motor Company Research and Development Center for the use of their PHI 660 Scanning Auger Microprobes. Additional thanks go to the Electron Microbeam Analysis Laboratory and staff at the University of Michigan. Finally, thanks go out to S.M. Bruemmer at Pacific Northwest Laboratory for his support. This research was supported by the U.S. Department of Energy under grant DE-FG02-93ER-12310, by the Associated Western Universities-Northwest under U.S. Department of Energy grant DE-FG02-89ER-7552, by the Division of Materials Sciences, U.S. Department of Energy under contract DE-AC05-84OR21400 with Lockheed Martin Energy Systems, and by the Southeast Universities Research Association, Inc through the SURA/ORNL summer research program. Research partially supported by the Division of Materials Sciences, U.S. Department of En-

ergy under contract DE-AC05-96OR22464 with Lockheed Martin Energy Research Corp., through the SHaRE Program under contract DE-ACo5-76OR00033 with Oak Ridge Associated Universities. Partial support for T.R. Allen was provided by a National Science Foundation Graduate Fellowship.

References

[1] G.S. Was and P. Andresen, J. Metals 44(4) (1992) 8.
[2] D.L. Damcott, T.R. Allen and G.S. Was, J. Nucl. Mater. 225 (1995) 97.
[3] S. Dumbill and T.M. Williams, Proc. Conf. on Materials for Nuclear Reactor Core Applications, Vol. 1 (BNES, London, 1987) p. 119.
[4] S. Watanabe, H. Kinoshita, N. Sakaguchi and H. Takahashi, J. Nucl. Mater. 226 (1995) 330.
[5] S.M. Bruemmer, M.D. Merz and L.A. Charlot, J. Nucl. Mater. 186 (1991) 13.
[6] S. Dumbill, Ph.D. Thesis, University of Birmingham (1992).
[7] P.R. Okamoto and L.E. Rehn, J. Nucl. Mater. 83 (1979) 2.
[8] F.A. Garner and A.S. Kumar, in: Radiation-Induced Changes in Microstructure: 13th Int. Symp. (Part I), ASTM STP 955, eds. F.A. Garner, N.H. Packan and A.S. Kumar (American Society for Testing and Materials, Philadelphia, 1987) pp. 289–314.
[9] W.G. Johnston, T. Lauritzen, J.H. Rosolowski and A.M. Turkalo, in: Radiation Damage in Metals (American Society of Metals, Cleveland, OH, 1976) pp. 227–266.
[10] H. Venker and K. Erlich, J. Nucl. Mater. 60 (1976) 347.
[11] J.M. Perks, A.D. Marwick and C.A. English, A computer code to calculate radiation-induced segregation in concentrated ternary alloys, AERE Report R 12121 (1986).
[12] B. Million, J. Ruzickova and J. Vrestal, Mater. Sci. Eng. 72 (1985) 85.
[13] T.R. Allen, D.L. Damcott, G.S. Was and E.A. Kenik, in: Proc. Seventh Int. Symp. on Env. Deg. of Materials in Nuclear Power Systems-Water Reactors, ed. R.E Gold and E.P Simonen, Breckenridge, CO, 1995, p. 997.
[14] M.J. Norgett, M.T. Robinson and I.M. Torrens, Nucl. Eng. Des. 33 (1974) 50.
[15] S.J. Rothman, L.J. Nowicki and G.E. Murch, J. Phys. F: Met. Phys. 10 (1980) 383.
[16] R.W. Seigel, in: Point Defects and Interactions in Metals, ed. Takamura (North-holland Pub. Co.) p. 533.
[17] M. Kiritani and H. Tanaka, J. Nucl. Mater. 69–70 (1978) 277.
[18] C. Dimitrov and O. Dimitrov, J. Phys. F: Met. Phys. 14 (1984) 793.
[19] N.Q. Lam, A. Kumar and H. Wiedersich, in: Effects of Radaition on Materials: Eleventh Conf., ASTM STP 782, eds. H.R. Brager and J.S. Perrin (American Society for Testing and Materials, 1982) pp. 985–1007.
[20] R.D. Carter, D.L. Damcott, M. Atzmon, G.S. Was and E.A. Kenik, J. Nucl. Mater. 205 (1993) 361.
[21] G.S. Was and T. Allen, J. Nucl. Mater. 205 (1993) 332.
[22] R.D. Carter, D.L. Damcott, M. Atzmon, G.S. Was, S.M. Bruemmer and E.A. Kenik, J. Nucl. Mater. 211 (1994) 70–84.
[23] J. Walmsley, P. Spellward, S. Fisher and A. Jenssen, in: Proc. Seventh Int. Symp. on Env. Deg. of Materials in Nuclear Power Systems-Water Reactors, eds. R.E Gold and E.P Simonen, Breckenridge, CO, 1995, p. 985.
[24] F.A. Garner, H.R. Brager, R.A. Dodd and T. Lauritzen, Nucl. Instrum. Meth. Phys. Res. B 16 (1986) 244.
[25] T.R. Allen and G.S. Was, Proc. Mater. Res. Soc. Symp., Vol. 373 (Materials Research Society, Pittsburgh, 1995) p. 101.
[26] J.P. Cenedese, F. Bley and S. Lefebvre, Acta Crystall. A40 (1984) 228.
[27] A.D. Marwick, R.C. Pillier and T.E. Cranshaw, J. Phys. F. Met. Phys. 17 (1987) 37.
[28] A. Marucco, Mat Sci. Eng. A189 (1994) 267.
[29] C. Dimitrov, D. Huguenin, P. Moser and O. Dimitrov, J. Nucl. Mater. 174 (1990) 22.